Geomorphology 403 (2022) 108178

Contents lists available at ScienceDirect

Geomorphology

journal homepage: www.journals.elsevier.com/geomorphology

# Particle size effect on geochemical composition of experimental soil mixtures relevant for unmixing modelling

Leticia Gaspar [a,*], William H. Blake [b], Ivan Lizaga [a,c], Borja Latorre [a], Ana Navas [a]

[a] Soil and Water Department, Estación Experimental de Aula Dei (EEAD-CSIC), Zaragoza, Aragón E-50059, Spain
[b] School of Geography, Earth and Environmental Sciences, University of Plymouth, Plymouth, Devon PL4 8AA, UK
[c] Isotope Bioscience Laboratory - ISOFYS, Department of Green Chemistry and Technology, Ghent University, Coupure Links 653, 9000, Gent, Belgium

ARTICLE INFO

*Keywords:*
Particle size distribution
Geochemical tracers
Specific surface area
Sediment Fingerprinting
Unmixing modelling
FingerPro

ABSTRACT

Sediment fingerprinting experiments have been used to demonstrate the sensitivity of numerical mixing model outputs to different particle size distributions in source materials and experimental sediment mixtures. The study aims to examine further grain size effects in the distribution of geochemical elements by soils through a laboratory experiment simulating mixing and sorting processes, to investigate if different size fractions are influencing fingerprinting analyses and unmixing model results. Multiple particle size fractions are analysed to understand the relationship between particle size and source signal through elemental signatures. FingerPro model was applied to unmix six experimental mixtures with known percentages contribution from three experimental sources. The experimental design comprised four different setups with a specific size fraction for sources (S) and mixtures (M). Setups A (S <63 and M <63 μm) and B (S <20 and M <20 μm) relies upon a comparable particle size fraction for sources and mixtures, while C (S <63 and M <20 with PSC) and D (S <63 and M <20) address particle size impacts simulating fine enrichment, with and without a single particle size correction factor, respectively. Tracers were extracted after applying two statistical tests, the range test (RT) and a combination of RT, Kruskal-Wallis (KW) and DFA tests thus obtaining the set of optimum tracers for each mixture. Our findings indicate that source apportionment results are sensitive to tracer selection and particle size. The most accurate source apportionment results were achieved when comparing sources and mixtures with the <63 μm grain-size fraction (setup A) by using the set of tracers extracted after RT, KW and DFA tests, (mean RMSE: 2%, AE: 2%). Larger errors were obtained progressively for setups B, C and D with better results when using more number of tracers from RT (mean RMSE: 7, 10, 13%, AE: 8, 11, 15%, respectively). The main strength of using experimental mixtures with a known contribution of the sources relies on reducing the uncertainty of the unmixing model outputs, one of the main limitations in fingerprint studies. The impact of SSA on the elemental concentration is difficult to predict because the positive linearity between them does not apply equally to all elements and this assumption needs to be constantly examined and considered for fingerprinting studies. Otherwise, the use of a single particle size correction factor could negatively affect unmixing results. The outcomes of this research will help to develop appropriate strategies for sediment fingerprinting, contributing to our knowledge of processes affecting sediment geochemistry and sediment transport across different particle sizes.

## 1. Introduction

Discriminating the potential contribution from sediment sources is necessary for understanding river basin sediment delivery and to support conservation of soil and water resources and catchment and reservoir management strategies (Navas et al., 2009, 2011). In this context, the sediment fingerprinting technique can provide information to help identify and quantify the source of mobilised sediments in agroforestry catchments (Lizaga et al., 2021) as agricultural uses have been identified as main contributors to sediment supply in a variety of environments (Blake et al., 2012; Collins et al., 2012; Reiffarth et al., 2016; Pulley and Collins, 2018). The occurrence of intense soil erosion and subsequent transport of fine eroded particles in surface waters increase sediment delivery (Palazón et al., 2016) especially after heavy rainfalls (Gaspar et al., 2019a). Drylands worldwide where fragile and degraded soils are subjected to intense rainfall, especially bare surfaces,

* Corresponding author.
*E-mail address:* lgaspar@eead.csic.es (L. Gaspar).

https://doi.org/10.1016/j.geomorph.2022.108178
Received 7 October 2021; Received in revised form 16 February 2022; Accepted 16 February 2022
Available online 21 February 2022

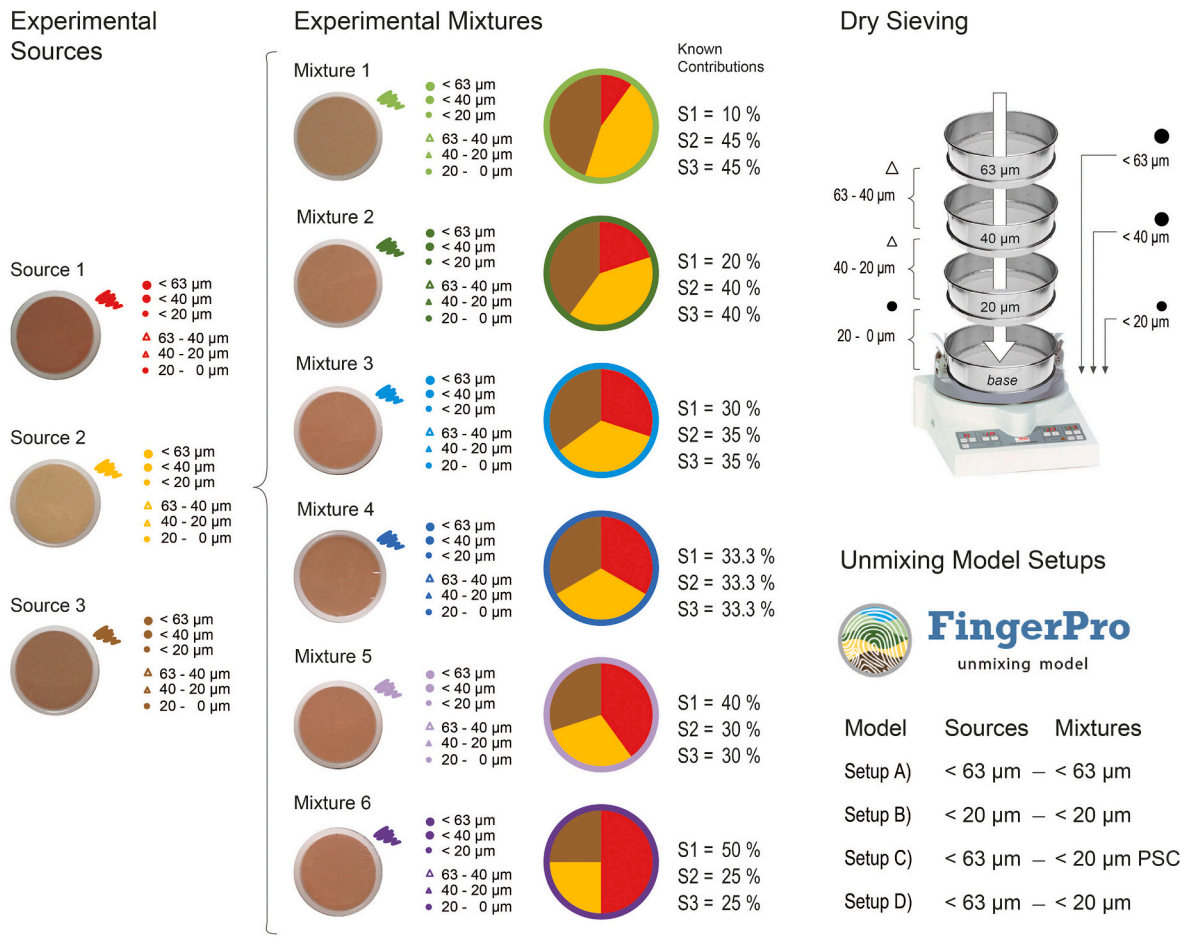


**Fig. 1.** Lab sampling design using 6 experimental mixtures with known relative contribution from 3 experimental sources for different particle size fractions: <63 µm, <40 µm, <20 µm (20–0 µm), 63–40 µm, 40–20 µm. Note that the fraction < 20 µm and the fraction 20–0 µm are the same samples.

**Table 1**
Basic statistics of the elemental composition (ppm) and size fractions for all experimental samples analysed in the fractions 63–40, 40–20, 20–0 µm: 3 sources (S1, S2, S3) and 6 mixtures (M1, M2, M3, M4, M5, M6) with three replicates for each sample ($n = 81$).

| | Mean | SD | CV % | Error | Min | Max |
|---|---|---|---|---|---|---|
| Si | 265,920.0 | 18,215.1 | 6.8 | 2,023.9 | 237,627.0 | 317,896.0 |
| Al | 66,708.3 | 9,172.7 | 13.8 | 1,019.2 | 44,976.3 | 91,542.0 |
| Fe | 39,713.2 | 6,252.0 | 15.7 | 694.7 | 27,854.3 | 55,276.1 |
| K | 28,089.4 | 4,542.6 | 16.2 | 504.7 | 16,760.5 | 39,298.3 |
| Ti | 7,156.7 | 976.5 | 13.6 | 108.5 | 4,483.5 | 9,316.8 |
| P | 2,047.6 | 189.8 | 9.3 | 21.1 | 1,403.6 | 2,512.9 |
| Mg | 3,391.7 | 837.6 | 24.7 | 93.1 | 2,350.6 | 6,622.1 |
| Ca | 2,761.1 | 1,111.4 | 40.3 | 123.5 | 953.9 | 5,790.0 |
| Zr | 386.1 | 57.3 | 14.8 | 6.4 | 269.1 | 527.3 |
| Sr | 171.5 | 84.4 | 49.2 | 9.4 | 58.1 | 405.9 |
| Rb | 144.7 | 22.0 | 15.2 | 2.4 | 93.6 | 204.7 |
| V | 135.7 | 24.7 | 18.2 | 2.7 | 59.8 | 198.4 |
| Cr | 106.7 | 27.4 | 25.7 | 3.0 | 55.7 | 173.0 |
| Zn | 96.5 | 27.9 | 28.9 | 3.1 | 48.4 | 202.0 |
| Pb | 53.9 | 14.4 | 26.8 | 1.6 | 17.6 | 85.8 |
| Nb | 23.8 | 3.4 | 14.3 | 0.4 | 15.8 | 31.8 |
| Clay % | 3.7 | 0.5 | 13.1 | 0.1 | 2.9 | 5.0 |
| Silt % | 94.7 | 2.1 | 2.2 | 0.2 | 88.4 | 97.0 |
| Sand % | 1.6 | 1.9 | 120.9 | 0.2 | 0.1 | 7.1 |

are highly susceptible to soil loss. In such conditions, the main driving factors and sources of fine particle export appear closely related to land use, especially agriculture which has been determined by using fingerprinting techniques to be the dominant source of suspended sediments in many river basins (Nosrati et al., 2018; Lizaga et al., 2020a).

Hydrological and fluvial sorting of eroded soil particles is an important consideration in the study of sediment transport processes. The influence of particle size on sediment source signals is widely recognised, though moderately few studies have focused on tracing different particle size fractions (e.g., Motha et al., 2002; Hatfield and Maher, 2009; Haddadchi et al., 2015). Differences in grain size on soil and sediments can bias fingerprint property data, triggering the direct comparison of source and target sediment samples to be incorrect. To date, this question has been addressed by fractionating the samples, typically using the <63 µm (e.g. Walling et al., 1993) or < 10 µm (Douglas et al., 2003) fractions, and by using particle size correction factors (e.g. Collins et al., 1997; Foucher et al., 2015). A further understanding of the relationship between particle size and elemental concentration is essential to improve the knowledge of sediment tracer predictability (Laceby et al., 2017).

The current recommended method for evaluating un-mixing model predictions is the use of artificial or virtual sample mixtures (Collins et al., 2017; Gaspar et al., 2019b; Uber et al., 2019). Accordingly, mixture tests have become increasingly established in recent studies (e.g., Haddadchi et al., 2015; Blake et al., 2018; Mohammadi Raigani et al., 2019; Nosrati et al., 2019; Collins et al., 2020).

In order to minimised issues of differences in grain size distribution between source and sediment in fingerprinting studies, the analyses are often limited to the <63 µm grain-size fraction, which seems to comprise the bulk of suspended sediments (Walling et al., 2000) and seems to be less susceptible to particle size processes (Koiter et al., 2018).

In order to mitigate particle size effects on tracers, there are two

**Table 2**
Pearson correlation coefficients (r) between elements (ppm) and size fractions for all experimental samples analysed in the fractions 63–40, 40–20, 20–0 μm (n = 81). The correlation matrix has been reordered according to the correlation coefficient. Background colors mean P-value <0.05 with a confidence level of 95%: dark red (r Pearson > 0.65), light red (r Pearson < 0.65), dark blue (r Pearson > −0.65), light blue (r Pearson < −0.65).

| | K | Fe | Zr | Cr | Rb | Sr | Al | V | Silt | Nb | Ti | Si | Clay | Sand | Mg | Zn | Ca | P |
|---|---|---|---|---|---|---|---|---|---|---|---|---|---|---|---|---|---|---|
| Pb | 0.8 | 0.7 | -0.1 | 0.5 | 0.5 | 0.4 | 0.2 | 0.1 | -0.1 | -0.3 | -0.4 | -0.7 | -0.2 | 0.1 | 0.4 | 0.5 | 0.6 | 0.5 |
| K | | 0.8 | 0.0 | 0.6 | 0.7 | 0.5 | 0.3 | 0.2 | 0.2 | 0.0 | -0.1 | -0.6 | -0.1 | -0.2 | 0.5 | 0.5 | 0.6 | 0.5 |
| Fe | | | 0.1 | 0.9 | 0.9 | 0.9 | 0.7 | 0.6 | 0.3 | 0.1 | 0.1 | -0.7 | -0.6 | -0.2 | -0.1 | 0.0 | 0.1 | 0.2 |
| Zr | | | | 0.0 | 0.0 | 0.1 | 0.0 | 0.0 | -0.1 | 0.0 | -0.2 | -0.2 | -0.4 | 0.2 | -0.2 | -0.3 | -0.1 | 0.0 |
| Cr | | | | | 0.9 | 0.8 | 0.8 | 0.7 | 0.5 | 0.3 | 0.4 | -0.5 | -0.6 | -0.4 | -0.2 | -0.1 | 0.0 | 0.1 |
| Rb | | | | | | 0.9 | 0.9 | 0.7 | 0.7 | 0.5 | 0.4 | -0.4 | -0.6 | -0.6 | -0.1 | -0.1 | -0.1 | 0.1 |
| Sr | | | | | | | 0.9 | 0.8 | 0.6 | 0.4 | 0.4 | -0.6 | -0.9 | -0.4 | -0.5 | -0.4 | -0.4 | -0.2 |
| Al | | | | | | | | 0.8 | 0.8 | 0.6 | 0.7 | -0.2 | -0.7 | -0.7 | -0.4 | -0.3 | -0.4 | -0.1 |
| V | | | | | | | | | 0.6 | 0.6 | 0.6 | -0.2 | -0.6 | -0.5 | -0.4 | -0.3 | -0.4 | -0.2 |
| Silt | | | | | | | | | | 0.8 | 0.8 | 0.2 | -0.5 | -0.9 | -0.3 | -0.3 | -0.3 | -0.1 |
| Nb | | | | | | | | | | | 0.9 | 0.4 | -0.3 | -0.8 | -0.3 | -0.3 | -0.4 | -0.1 |
| Ti | | | | | | | | | | | | 0.4 | -0.2 | -0.8 | -0.4 | -0.3 | -0.5 | -0.2 |
| Si | | | | | | | | | | | | | 0.5 | -0.3 | 0.1 | 0.0 | -0.2 | 0.0 |
| Clay | | | | | | | | | | | | | | 0.3 | 0.7 | 0.6 | 0.6 | 0.4 |
| Sand | | | | | | | | | | | | | | | 0.1 | 0.1 | 0.2 | 0.0 |
| Mg | | | | | | | | | | | | | | | | 0.8 | 0.8 | 0.6 |
| Zn | | | | | | | | | | | | | | | | | 0.9 | 0.6 |
| Ca | | | | | | | | | | | | | | | | | | 0.7 |

principal approaches in sediment tracing studies comprising: i) using fine particle size sub-fractions (e.g., of the <63 μm fraction) selected carefully on the basis of the d90 particle size for the target sediment samples, and ii) the use of more generic broader particle size fractions (e.g., the bulk <63 μm fraction) combined with further correction factors in the un-mixing model (Collins et al., 2017; Laceby et al., 2017; Gaspar et al., 2019b).

Differences in grain size composition between source and mixture are likely to result in differences in tracer property concentrations limiting the reliability of fingerprinting techniques in some circumstances. Different approaches have been applied during the last decades to tackle this, for example using particle size correction factors, most of them based on the ratio of specific surface area (SSA). Nevertheless, there is debate in the literature on whether the particle size correction (PSC) factor is appropriate or not (Laceby et al., 2017; Smith et al., 2018; Collins et al., 2020; Nosrati et al., 2021). The PSC factor is based on the enrichment in the fine particles, assuming that the relation between the specific surface area and tracers is linear and is the same for all the potential tracers. Most particle size correction factors assume that the relation between both particle size and fingerprint concentrations is similar for all fingerprints. There is evidence that these assumptions may not be met in many cases (Smith et al., 2018; Gholami et al., 2019) and that data correction can result unsatisfactory (Russell et al., 2001).

To address these issues, comparison of estimated source contributions of experimental mixtures with known composition and contribution, is of value to develop relationships for improving our understanding on the particular effect of grain size on the elemental composition of sediment mixtures. In this context, undertaking source fingerprinting using different size fractions could ensure that any potential errors arising from particle size controls on tracers will be minimised by testing different unmixing model setups. Understanding sorting controls on measured elemental concentration may also allude to influence of sorting effects on delivery dynamics of sediment-associated contaminants.

In this study, an experimental approach using artificial mixtures and modelling has been integrated to evaluate the impact of the particle size variability on soil provenance when using fingerprinting unmixing models. The objectives are to i) analyse the behaviour of stable elements in soils and sediment mixtures for different size fractions, ii) test the effect of the particle size variability of soil and sediments on estimates of soil apportions by using artificial mixtures, and iii) compare with results of an unmixing model assuming conservative behaviour of soils (i.e. not affected by sorting processes). Our study aims to provide insights of value for accounting for grain size effects when interpreting elemental geochemistry composition in soil and sediment.

## 2. Material and methods

### 2.1. Laboratory procedures

A brief summary of the experimental design is schematically shown in Fig. 1. Three natural soils were selected as experimental sources. These soils belong to a similar sedimentary substrate and were characterised by a singular elemental composition to have good discrimination between them following the fingerprint methodological framework. Sources were sieved to 2 mm and them a set of six experimental mixtures were created by mixing a different known relative contribution of the three experimental sources, producing three replicates per sample (Fig. 1). All samples were dried, gently disaggregated using a mortar and pestle, fractionated and subdivided into 5 different fractions by dry sieving: 63–0 μm (<63 μm), 40–0 μm (<40 μm), 20–0 μm (<20 μm), 63–40 μm and 40–20 μm. The dry-sieving protocol consisted of shaking the soil samples placed on top of a nest of sieves (63, 40, and 20 μm; 20 cm Ø) for 25 min at ~200 rotation $min^{-1}$. Soil retained on the 40 and 20 μm sieves were considered as 63–40 and 40–20 μm soil fractions, respectively. The soil collected in the cup under the 20 μm sieve was the <20 μm soil fraction which coincides with the fraction 20–0 μm. Soil aliquots were taken directly from each sieve for elemental analysis and used to measure soil fractions' distributions.

Elemental geochemistry was analysed by X-ray fluorescence (XRF) using a Thermo Fisher Scientific Niton XL3T 950 He GOLDD XRF analyser, equipped with different excitation filters (main, low and high range) that optimise the analyser's sensitivity for various elements. The instrument was calibrated with reference materials, helium was used to allow measurement of light elements, and low drift, less than 1%, was recorded during the analysis. Samples were packed into XRF sample cups with a 38.2-mm exposure diameter in which the laser pulse (3-mm diameter) strikes the surface of the sample. The elemental composition

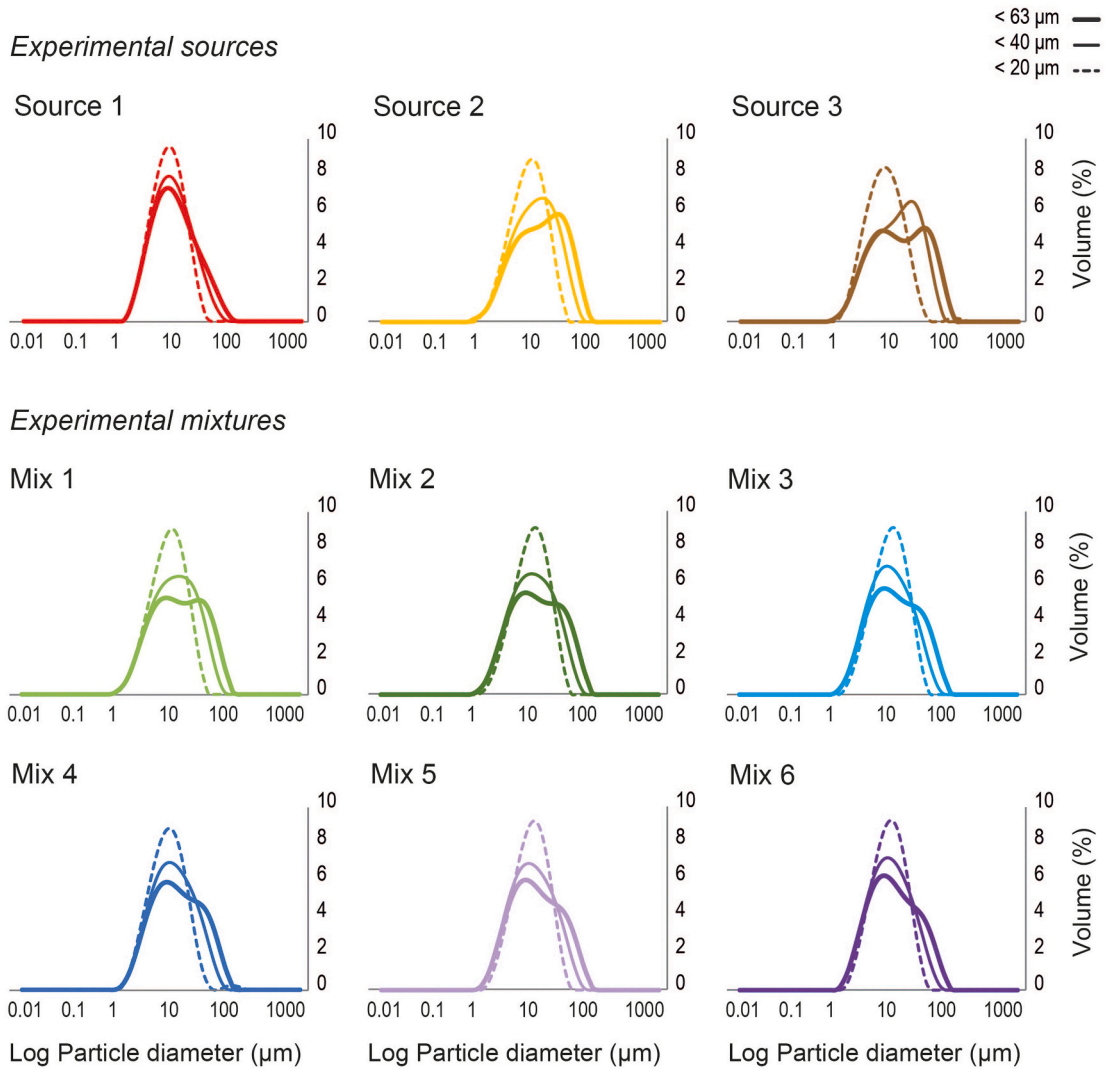


**Fig. 2.** Particle size distribution by laser diffraction for all experimental samples and mixtures analysed in <63 µm, <40 µm, <20 µm fractions ($n$ = 81). a) Granulometric curves obtained by averaging data from the corresponding 25 measurement runs during representative pump speed steps per sample, b) bar plot of sand, silt and clay content (%) for the three different fractions (<63 µm, <40 µm, <20 µm) for each experimental sample.

of experimental sources and mixtures was measured at each size fraction, obtaining a dataset of 135 measurements. Despite a total of 27 elements were analysed, only 16 elements returned measurements above the limit of detection: Al, Ca, Cr, Fe, K, Mg, Nb, P, Pb, Rb, Si, Sr, Ti, V, Zn and Zr.

The particle size composition and size distribution of each experimental sample (3 sources and 6 mixtures) was measured by using a 2000 series laser granulometer analyser (Malvern, UK) and corresponding values of mean specific surface area were estimated for each fraction. A sub-sample was digested in hydrogen peroxide over 24 h to remove organic matter and disaggregated in an ultrasonic bath prior to particle size analysis. Particle size data were used to calculate the specific surface area (SSA, $m^2\ g^{-1}$) by assuming particle sphericity (Smith and Blake, 2014).

### 2.2. Experimental design

This study is based on experimental samples and laboratory procedures, which means that the effect of natural processes like any geochemical transformations during fluvial erosion and transportation are not considered. However, the sorting process has been reproduced by taking it to the limit with setup C and D, where sources (<63) and mixtures (<20) have different size fractions, simulating fine particle enrichment in suspended sediment.

The relative contributions from the three sources were calculated using the multivariate mixing model FingerPro (Lizaga et al., 2020b). The range test alone (RT) and the combination of RT, KW and DFA tests were used to identify the list of elements selected as two independent sets of optimum composite fingerprint properties. The fingerprinting procedure used for comparing the quantitative source ascription obtained with variations in size fractions involved four setups for the unmixing model:

A) comparing sources and mixtures at <63 µm
B) comparing sources and mixtures at <20 µm
C) comparing sources at <63 µm and mixtures at <20 µm with particle size correction factor (PSC)
D) comparing sources at <63 µm and mixtures at <20 µm without PSC factor.

In this study, the optimised solution among the four model setups was obtained by comparing the root mean squared error (RMSE) between the predicted and known apportionments used to create the experimental mixtures in the lab. In addition, the accuracy of each

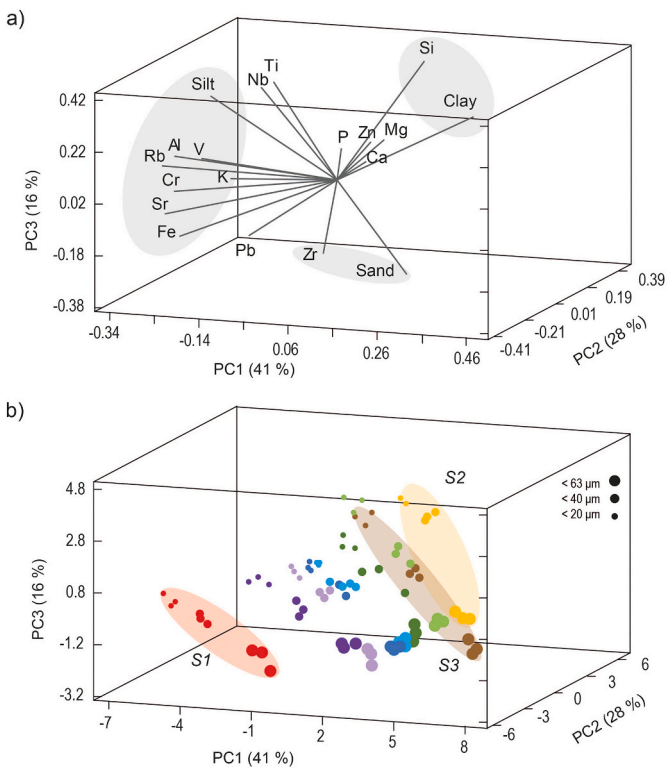


**Fig. 3.** Principal components analysis (PCA): a) score 3D plot and b) loading biplot of the principal components (PC1, PC2 and PC3) for all experimental samples and mixtures analysed in the <63 μm, <40 μm, <20 μm fractions (n = 81).

source contributions was evaluated with the absolute value of the difference between the known and estimated contributions, absolute error (AE), obtaining a standard deviation (SD) value for the four samples simulates, three replicates as experimental mixtures and the average of the three replicates as artificial mixture. The heterogeneity of each source is considered as a t-distribution for each property, and the fingerprinting analysis of each mixture using FingerPro model is repeated by randomly sampling the source probability distributions (e.g. 1000 iterations).

The particle size correction factor used in this study is based on the ratio of the specific surface area (SSA) of the experimental mixtures and source samples and this value is then multiplied by the fingerprint concentration for each source (Collins et al., 1997; Walling, 1998). The source discrimination analyses before the unmixing were done separately for each of the size fractions, each mixture and each unmix setup.

## 3. Results

### 3.1. Concentration and particle size

A summary of the elemental composition for source and mixtures in different size fractions is listed in Table 1. The group of elements that were correlated with *r Pearson* higher than 0.65 included Al, Fe, and K, a second group consisting of Mg, Ca and P and another group formed by Sr, Rb, V and Cr. Aluminium in turn, was significantly and positively correlated with Ti, Sr, Rb, V and Cr, while Fe was correlated with Sr, Rb, V, Cr and Pb. Other highly significant correlations were between Nb with Ti, or Zn with Mg and Ca. Silicon was negatively correlated with most elements, reaching the highest significance with Fe and Pb, although it was positively but moderately correlated with Ti and Nb (Table 2).

The soil texture of the sources and mixtures samples was mainly silty loam, with a predominance of the silt fraction ranging between 56 and 86%. The grain size distribution curves (Fig. 2) showed differences between the different fractions, except for sample S1, which presented a normal distribution for all of them. A unimodal distribution with one clear peak was evident in the smaller size fraction (<20 μm). In comparison, higher dispersion was observed for the bigger particle sizes, in which a bimodal distribution was even observed for the fraction <63 μm in S3. Differences were also observed when comparing the granulometric curves of the three sources; both the dispersion of the curves and the content of larger particles (<63 μm) progressively increased from S1 to S3. Similar curves were observed between the mixtures for all fractions.

The scatter plot of the three principal components in the PCA analysis for the fractions showed a clear difference between elements occupying different parts of the diagram (Fig. 3). Three components with eigenvalues greater than 1 explained 84.6% of the variations of sources and mixtures. On one side, Al, Fe, Sr, Rb, Cr, V, Ti, Nb and silt directly correlated between them and included in component 1, explained 41.1% of the total variance. In the second component Si, P, Mg, Ca, Zn and clay also directly correlated accounted for 27.9% of the total variance, while in component 3 (15.6%) Al, Ti, Nb were inversely correlated with sand.

Significant differences were found in the mean concentration of most elements between the three sources. Source S1 was characterised by significantly higher mean contents of Al, Fe, Cr, V, Sr, Zr and Rb in comparison with their means in the other two sources, while S2 presented significant higher mean content of Si and significant lower contents of K and Pb than S1 and S3. Source S3 was characterised by significant higher mean contents of Ca, Mg, Zn, P, Nb and significant lower mean content of Ti (Fig. 4).

On the other hand comparing between different fractions in terms of abundance, the elemental composition varied according to the particle size fraction (Tables 3 and 4). In general, except for S2, mean contents of Al, Fe, K, Sr and Rb were significantly different in each fraction, with the higher contents in the finer fraction (20–0 μm) and the lower in the coarser one (63–40 μm). Similar results were also recorded in the mean contents of Ti, Cr, Zn and Pb only for S3. However, despite these general findings, an opposite pattern was identified for Zr content, that significantly and progressively increased from the finer to the coarser fractions.

In the fractions <63, <40 and <20 μm, the specific surface area varied from 3.20 to 4.43 $m^2\ g^{-1}$ with significant differences between the means (means: 3.36, 3.57 and 4.07 $m^2\ g^{-1}$ for <63, <40 and <20 μm, respectively). Fig. 4 depicts the relationships between the elemental composition and specific surface area for sources S1, S2 and S3 that can be expressed as linear functions. Correlation analysis also indicates that there was a strong linear relationship between the content of Al, K, Ti, Sr and Rb with SSA, increasing their contents with an increase in the specific surface area. This relationship was consistent for elements like Cr, Zn, Fe and Pb in S1 and S3 samples, for Mg and Nb only in S3 and for Ca in S1 samples. However, the content of Zr in all samples and the content of Fe in source S2 decreased significantly when SSA increased ($r^2 = -0.98$).

In Fig. 5, the general trends from lowest to highest specific surface area in each experimental mixture showed a significant increase in most elements. The stronger correlation coefficients, higher than 0.8, were found for Al, K, Ti, Sr, Rb in all mixtures and for Fe only in mixtures M4, M5 and M6 (Fig. 5). Rather poor results were obtained for elements like Mg and Pb while strong but negative correlations were recorded between the SSA and the content of Zr in all mixtures, and with the content of P in M3 and M6. Elements like Ca and Si showed strong but both positive and negative correlations with SSA depending on the experimental mixture analysed. Thus, significant direct correlations were found between Si and SSA in M2 and M3 but negative in M6, while for Ca correlations were direct in M1 and M4 but negative in M3 (Fig. 5).

Along with the type of Pearson correlations (Fig. 5) we can conclude

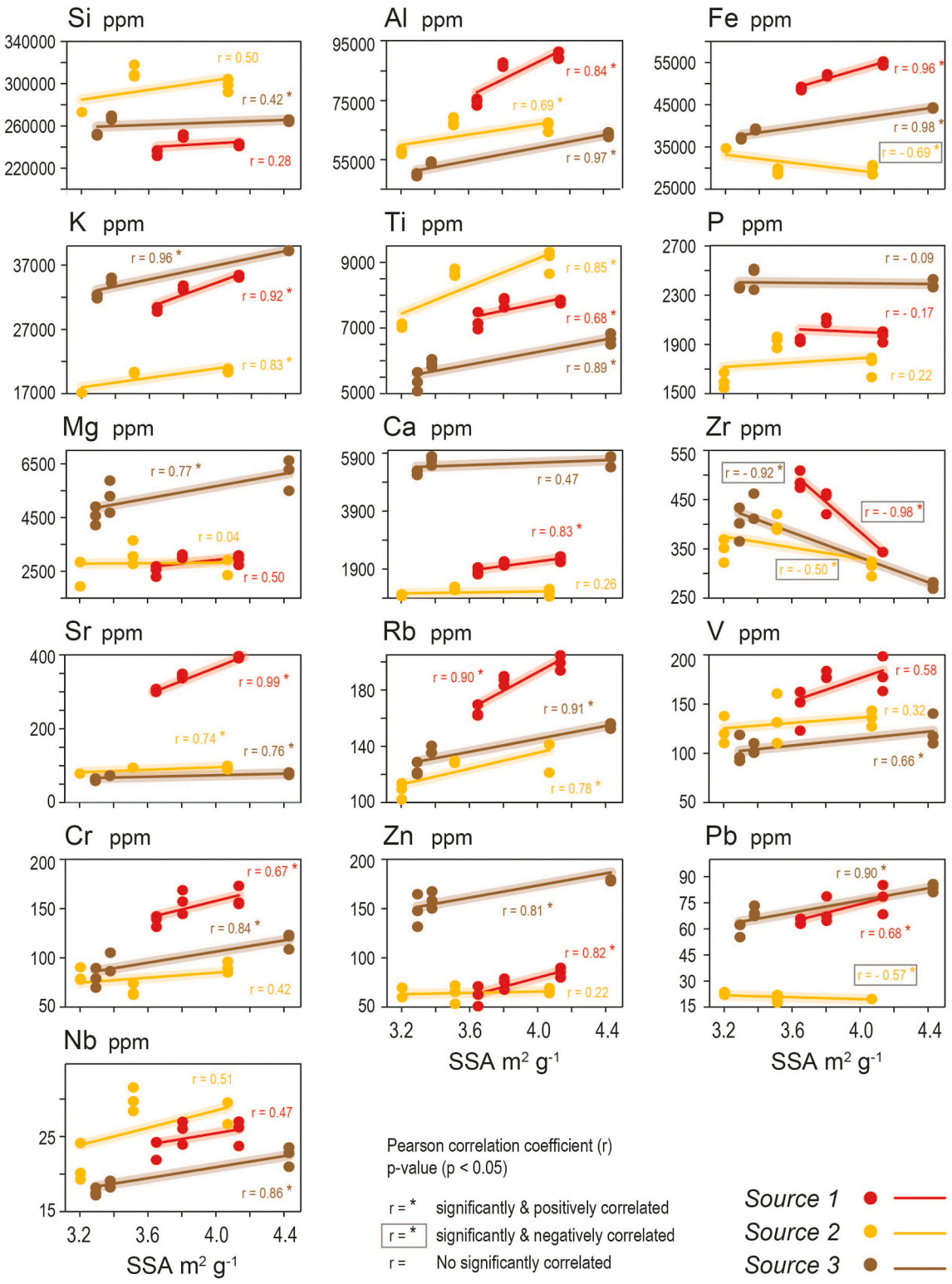


**Fig. 4.** Scatter plot of specific surface area (SSA, $m^2\ g^{-1}$) versus element contents (ppm) with linear regression trendlines for each of the three sources.

that Al, K, Ti, Sr and Rb were enriched (average, 20, 18, 21, 32 and 23%) respectively, in the <20 μm fraction compared to the <63 μm fraction. Elements like Mg, Cr, Zn and Nb also registered enrichment in the <20 μm fraction up to 20, 14, 30, 33 and 28%, respectively, but only for some of the experimental samples. P and V were not affected by grain size, Our findings also recorded an opposite trend for the Zr content in all samples and for Pb in S2 and the mixtures M2 and M6, with average enrichment in the <63 μm fraction of 25 and 14% respectively. The content of Fe encompassed different enrichment patterns in the <20 μm fraction for S1, S2, M4, M5, M6 and in the <63 μm fraction for S2. In addition, the content of Ca was enriched in the <20 μm fraction in S1, M1 and M4, but had an opposite pattern in M3, while no significant control of SSA was exerted for S2, S3, M2, M5 and M6.

For all the sources and mixtures the percentage of the variation explained by a best-fit regression linear model between specific surface area (SSA) and element content (ppm) with a confidence level of 95% (*P*-

**Table 3**
Least squares mean of each element content by i) fractions 63–40, 40–20, 20–0 μm and ii) fractions <63, <40, <20 μm, separately, for each experimental source. Asterisks and different letters indicate significant differences at the 95% confidence level between group.

| Fractions | | | | | | | | Fractions | | | | | | | |
|---|---|---|---|---|---|---|---|---|---|---|---|---|---|---|---|
| | *P*-value | | 63–40 μm | | 40–20 μm | | 20–0 μm | | *P*-value | | <63 μm | | <40 μm | | <20 μm | |
| Experimental source S1 | | | | | | | | | | | | | | | | |
| Si | 0.00 | * | 239,378 | a | 249,933 | b | 242,173 | a | 0.00 | * | 234,668 | a | 246,053 | c | 242,173 | b |
| Al | 0.00 | * | 76,822 | a | 86,996 | b | 90,010 | c | 0.00 | * | 74,528 | a | 88,503 | b | 90,010 | b |
| Fe | 0.00 | * | 49,297 | a | 51,969 | b | 54,851 | c | 0.00 | * | 48,911 | a | 53,410 | b | 54,851 | c |
| K | 0.00 | * | 30,473 | a | 33,415 | b | 35,222 | c | 0.00 | * | 30,211 | a | 34,319 | b | 35,222 | c |
| Ti | 0.00 | * | 7,019 | a | 7,787 | b | 7,815 | b | 0.01 | * | 7,194 | a | 7,801 | b | 7,815 | b |
| P | 0.00 | * | 1,912 | a | 2,101 | b | 1,965 | a | 0.30 | | 1,631 | a | 2,033 | a | 1,965 | a |
| Mg | 0.01 | * | 2,487 | a | 3,049 | b | 2,926 | b | 0.02 | * | 2,510 | a | 2,988 | b | 2,926 | b |
| Ca | 0.00 | * | 1,845 | a | 2,109 | b | 2,235 | b | 0.01 | * | 1,823 | a | 2,172 | b | 2,235 | b |
| Zr | 0.00 | * | 493 | c | 447 | b | 343 | a | 0.00 | * | 489 | c | 395 | b | 343 | a |
| Sr | 0.00 | * | 305 | a | 342 | b | 398 | c | 0.00 | * | 304 | a | 370 | b | 398 | c |
| Rb | 0.00 | * | 164 | a | 187 | b | 199 | c | 0.00 | * | 165 | a | 193 | b | 199 | b |
| V | 0.09 | | 157 | a | 179 | a | 180 | a | 0.08 | | 146 | a | 179 | b | 180 | b |
| Cr | 0.30 | | 142 | a | 157 | a | 161 | a | 0.02 | * | 138 | a | 159 | b | 161 | b |
| Zn | 0.08 | | 67 | a | 74 | ab | 85 | b | 0.01 | * | 61 | a | 80 | b | 85 | b |
| Pb | 0.03 | * | 57 | a | 70 | ab | 77 | b | 0.13 | | 65 | a | 74 | a | 77 | a |
| Nb | 0.24 | | 24 | a | 26 | a | 26 | a | 0.22 | | 24 | a | 26 | a | 26 | a |
| Experimental source S3 | | | | | | | | | | | | | | | | |
| Si | 0.00 | * | 287,138 | a | 311,416 | c | 298,200 | b | 0.00 | * | 272,590 | a | 304,808 | b | 298,200 | b |
| Al | 0.00 | * | 59,194 | a | 66,979 | b | 65,990 | b | 0.00 | * | 57,291 | a | 66,485 | b | 65,990 | b |
| Fe | 0.03 | * | 27,986 | a | 29,242 | ab | 29,869 | b | 0.00 | * | 34,646 | b | 29,555 | a | 29,869 | a |
| K | 0.00 | * | 16,825 | a | 20,314 | b | 20,760 | b | 0.00 | * | 17,243 | a | 20,537 | b | 20,760 | b |
| Ti | 0.00 | * | 6,675 | a | 8,681 | b | 9,053 | b | 0.00 | * | 7,066 | a | 8,867 | b | 9,053 | b |
| P | 0.01 | * | 1,691 | a | 1,922 | b | 1,730 | a | 0.03 | * | 1,604 | a | 1,826 | b | 1,730 | ab |
| Mg | 0.42 | | 2,946 | a | 3,157 | a | 2,695 | a | 0.54 | | 2,551 | a | 2,926 | a | 2,695 | a |
| Ca | 0.45 | | 1,123 | a | 1,211 | a | 1,091 | a | 0.12 | | 983 | a | 1,151 | a | 1,091 | a |
| Zr | 0.00 | * | 354 | b | 401 | c | 311 | a | 0.05 | * | 347 | b | 356 | b | 311 | a |
| Sr | 0.00 | * | 78 | a | 95 | b | 94 | b | 0.00 | * | 78 | a | 95 | b | 94 | b |
| Rb | 0.00 | * | 99 | a | 129 | b | 135 | b | 0.02 | * | 109 | a | 132 | b | 135 | b |
| V | 0.36 | | 117 | a | 134 | a | 136 | a | 0.31 | | 123 | a | 135 | a | 136 | a |
| Cr | 0.01 | * | 64 | a | 67 | a | 90 | b | 0.14 | | 82 | a | 78 | a | 90 | a |
| Zn | 0.49 | | 80 | a | 63 | a | 66 | a | 0.72 | | 64 | a | 65 | a | 66 | a |
| Pb | 0.00 | * | 34 | b | 20 | a | 20 | a | 0.02 | * | 22 | b | 20 | a | 20 | a |
| Nb | 0.00 | * | 21 | a | 30 | b | 28 | b | 0.01 | * | 21 | a | 29 | b | 28 | b |
| Experimental source S3 | | | | | | | | | | | | | | | | |
| Si | 0.00 | * | 257,043 | a | 267,913 | b | 265,134 | b | 0.00 | * | 251,698 | a | 266,523 | b | 265,134 | b |
| Al | 0.00 | * | 46,192 | a | 53,910 | b | 63,472 | c | 0.00 | * | 49,751 | a | 58,691 | b | 63,472 | c |
| Fe | 0.00 | * | 31,993 | a | 39,063 | b | 44,252 | c | 0.00 | * | 37,086 | a | 41,657 | b | 44,252 | c |
| K | 0.00 | * | 30,096 | a | 34,531 | b | 39,243 | c | 0.00 | * | 32,193 | a | 36,887 | b | 39,243 | c |
| Ti | 0.00 | * | 4,777 | a | 5,923 | b | 6,662 | c | 0.00 | * | 5,358 | a | 6,292 | b | 6,662 | b |
| P | 0.30 | | 2,033 | a | 2,451 | a | 2,388 | a | 0.10 | | 2,361 | a | 2,419 | b | 2,388 | ab |
| Mg | 0.04 | * | 4,368 | a | 5,284 | ab | 6,135 | b | 0.02 | * | 4,562 | a | 5,709 | b | 6,135 | b |
| Ca | 0.00 | * | 4,776 | a | 5,649 | b | 5,650 | b | 0.02 | * | 5,239 | a | 5,650 | b | 5,650 | b |
| Zr | 0.02 | * | 443 | c | 436 | b | 277 | a | 0.00 | * | 400 | c | 356 | b | 277 | a |
| Sr | 0.00 | * | 61 | a | 73 | b | 78 | c | 0.00 | * | 62 | a | 76 | b | 78 | b |
| Rb | 0.00 | * | 114 | a | 137 | b | 155 | c | 0.00 | * | 123 | a | 146 | b | 155 | c |
| V | 0.02 | * | 77 | a | 104 | b | 123 | b | 0.27 | | 102 | a | 113 | a | 123 | ab |
| Cr | 0.00 | * | 66 | a | 96 | b | 118 | c | 0.00 | * | 79 | a | 107 | b | 118 | b |
| Zn | 0.00 | * | 115 | a | 159 | b | 186 | c | 0.03 | * | 148 | a | 172 | ab | 186 | b |
| Pb | 0.00 | * | 55 | a | 70 | b | 84 | c | 0.00 | * | 60 | a | 77 | b | 84 | c |
| Nb | 0.01 | * | 18 | a | 19 | a | 23 | b | 0.00 | * | 18 | a | 21 | b | 23 | b |

values < 0.05) ranged from 35% (Fe in M3) to 99% (Ti in M3). The linear models explained as much as 95% of the total variation of Zr in S1.

### 3.2. Unmixing model performance

In this section, experimental samples with granulometric ranges of <63 and <20 μm were used to perform comparisons for the four unmixing model setups: A, B, C and D. Corresponding DFA for each unmix setup achieved discrimination of 100% of sources and mixtures correctly classified. The first and second discriminant functions illustrated that sources were well separated and mixtures were spatially located within the sources except in the unmix setup D, which combined sources at <63 μm and mixtures at <20 μm (Fig. 6).

The list of elements used in the mixing models based on i) the range test (RT) and ii) the combination of RT, KW and DFA tests are listed in Table 5. Some differences were observed between the elements selected from RT, especially when comparing different unmix setups more than comparing the different mixtures. However, when using RT, KW and DFA no differences were observed between the elements selected that resulted in the identification of K, Sr and Rb as the optimum tracers for all mixtures and in all unmix setups, except for mix 6-D.

For comparisons between the <63 μm fraction for sources and mixtures (setup A), the RMSE ranged from 0.6 to 4.0% being the lowest errors compared with the other unmix setups (Table 6). The means of RMSE values for the two sets of tracers (RT and RT, KW, DFA, respectively) progressively increased from A (2.9 and 2.3%), B (7.5 and 13.3%), C (11.1 and 17.4%) and D (14.3 and 26.8%). The highest errors were obtained when comparing <63 μm for sources and <20 μm

**Table 4**
Least squares mean of each element content by i) fractions 63–40, 40–20, 20–0 μm and ii) fractions <63, <40, <20 μm, separately, for the experimental mixtures. Asterisks and different letters indicate significant differences at the 95% confidence level between groups.

| Fractions | | | | | | | | Fractions | | | | | | | |
|---|---|---|---|---|---|---|---|---|---|---|---|---|---|---|---|
| | *P*-value | | 63–40 μm | | 40–20 μm | | 20–0 μm | | *P*-value | | <63 μm | | <40 μm | | <20 μm | |
| Experimental mixtures | | | | | | | | | | | | | | | | |
| Si | 0.00 | * | 255,329 | a | 270,920 | b | 267,335 | b | 0.00 | * | 254,495 | a | 269,128 | bb | 267,335 | b |
| Al | 0.00 | * | 59,781 | a | 67,975 | b | 70,838 | c | 0.00 | * | 60,746 | a | 69,406 | b | 70,838 | b |
| Fe | 0.00 | * | 38,608 | a | 38,859 | a | 41,489 | c | 0.16 | | 39,914 | a | 40,174 | a | 41,489 | a |
| K | 0.00 | * | 26,170 | a | 27,655 | b | 29,098 | c | 0.00 | * | 26,107 | a | 28,376 | b | 29,098 | c |
| Ti | 0.00 | * | 6,190 | a | 7,326 | b | 7,957 | c | 0.00 | * | 6,437 | a | 7,642 | b | 7,957 | c |
| P | 0.02 | * | 2,029 | a | 2,115 | b | 2,038 | a | 0.11 | | 2,009 | a | 2,077 | b | 2,038 | ab |
| Mg | 0.40 | | 3,359 | a | 3,168 | a | 3,229 | a | 0.77 | | 3,299 | a | 3,198 | a | 3,229 | a |
| Ca | 0.00 | * | 2,877 | c | 2,480 | a | 2,786 | b | 0.50 | | 2,670 | a | 2,633 | a | 2,786 | a |
| Zr | 0.00 | * | 384 | b | 425 | c | 344 | a | 0.00 | * | 402 | c | 385 | b | 344 | a |
| Sr | 0.00 | * | 136 | a | 173 | b | 210 | c | 0.00 | * | 139 | a | 191 | b | 210 | b |
| Rb | 0.00 | * | 129 | a | 145 | b | 158 | c | 0.00 | * | 131 | a | 151 | b | 158 | c |
| V | 0.00 | * | 123 | a | 142 | b | 146 | b | 0.00 | * | 123 | a | 144 | b | 146 | b |
| Cr | 0.00 | * | 93 | a | 105 | b | 121 | c | 0.00 | * | 97 | a | 113 | b | 121 | b |
| Zn | 0.01 | * | 93 | a | 89 | a | 103 | b | 0.15 | | 93 | a | 96 | a | 103 | a |
| Pb | 0.00 | * | 59 | c | 49 | a | 56 | b | 0.00 | * | 62 | c | 52 | a | 56 | b |
| Nb | 0.00 | * | 20 | a | 25 | b | 26 | b | 0.00 | * | 21 | a | 26 | b | 26 | b |

mixtures (unmix setup D) that reached in mixtures 4 and 5 RMSE means of 29% with a set of 3 tracers.

In general, along with the increase of RMSE an increase in the mean absolute errors for source 1 occurred from unmix setup A, B, C to D for both sets of tracers (AE means using RT: 2.9, 5.3, 13.3, 19.0% and using RT, KW, DFA: 1.7, 4.8, 17.9, 37.0, respectively). Similarly trend was observed for source 2 with smaller mean AE for unmix setup A (3.0 and 2.3%) and higher for D (AE: 12.7 and 25%). On the other hand, for source S3 the highest AE was not recorded in setup D (when comparing <63 μm sources with <20 μm for mixtures) but in setup C. The means of AE progressively increased from A, D, B and C for both sets of tracers (AE means using RT: 3.6, 7.2, 9.2, 11.8 51% and using RT, KW, DFA: 2.2, 12.0, 17.8, 23.3%, respectively).

The accuracy of source contribution predictions varied between the sets of tracers, thus for unmix setup A slightly lower values of RMSE and AE were obtained when only three elements were selected as tracers after RT, KW and DFA tests. The opposite was observed for unmix setups B, C and D, where lower RMSE and AE values were estimated by using most of the elements selected from RT. For all simulations performed, the goodness of fit (GOF) values based on the sum of the squares of the relative errors were never less than 74% and 88% when using tracers selected from RT and RT, KW and DFA test, respectively.

The comparison of the predicted and known relative contributions from the three sources to the experimental and artificial mixtures in Fig. 7a and b, shows all the results for each mixture and each unmix setup. In general, higher variability in the predictions was observed when using the optimum tracers selected from RT (Fig. 7a) compared to more homogeneous results obtained when the combination of RT, KW and DFA tests was applied to select the optimum tracers (Fig. 7b).

## 4. Discussion

### 4.1. Concentration and particle size

The elemental content of the soil samples is the main driver of the geochemical differences found in the experimental sources, reflecting the composition of each sample. The distinctive elemental signatures are linked to the nature of parent materials and subsequent weathering, providing a good discrimination between the experimental sources, which is essential for quantifying their relative contributions to the experimental mixtures.

The list of elements that were highly correlated, besides the distribution of elements grouped in the first two principal components reflect that some elements such as Ca, Mg, Zn are likely associated with silicate minerals mainly contained in the clay fraction as suggested by their highest abundance in S3. In the case of the high content of Al, Fe, Sr, and Rb it is related to the minerals abundance in the silt fraction which is higher in S1.

Overall the positive correlations between specific surface area and elements like Al, K, Ti, Sr, Rb are consistent with most studies that also reported higher element enrichment in the fine fractions reflecting the increasing adsorption potential of larger SSA ($m^2\ g^{-1}$) (Horowitz and Elrick, 1987). For narrow ranges in SSA, Smith and Blake (2014) suggest that simple linear correlations may be a reasonable approximation, while for larger ranges of SSA (over 1 $m^2\ g^{-1}$), these relationships are often non-linear (Russell et al., 2001) or more complex (Horowitz, 1991; Foster et al., 1998).

However, the weak correlation between SSA and Mg, Fe, V, Cr, Zn in some mixtures and in S2, while a strong correlation is present in other mixtures might partly be controlled by the mineralogical composition in the soil source and particular elements bound within the fine soil components. Thus in accordance with records in a variety of soils on sedimentary materials, Fe, Zn and Cr appear strongly bound to minerals indicating its presence in the crystal lattices (Navas and Lindhorfer, 2003). However, other elements such as Mn can be associated to oxide phases (Wilcke et al., 1998). Besides, elements can have different associations to soil components depending on soil types, processes and parent materials (Navas and Lindhorfer, 2005).

Furthermore, our analysis shows an opposite trend than expected, with a strong negative correlation between SSA and Zr in most mixtures, and between SSA and Fe, Si and Ca in fewer mixtures. These relationships are likely strengthened by the fact that different adsorption of elements is determined not only by the specific surfaces of the soil but also by their composition, mineralogy and properties (Mandzhieva et al., 2014). The lack of correlation of Zr with any of the study elements and its segregation in the PCA suggests a different behaviour than the rest of elements, with a decreasing trend with SSA. Zircon is an accessory residual mineral that is common in many types of sediment and often resistant to more than one cycle of alteration (Wu and Zheng, 2004). In this regard Guagliardi et al. (2013) suggest that grain-size effects may contribute to a high zircon concentration in the <63 μm fraction.

An average increase of 22% of the specific surface area recorded in the very fine-grained particles (<20 μm) compared to the coarse one (<63 μm) for all experimental samples confirms that the smaller particles have higher SSA as described in the literature (e.g. Horowitz, 1991). However, the range of increase found in our experimental samples, which varies from 11 to 57%, reflects that the direct relation between SSA and size fraction is affected by the nature of each soil sample.

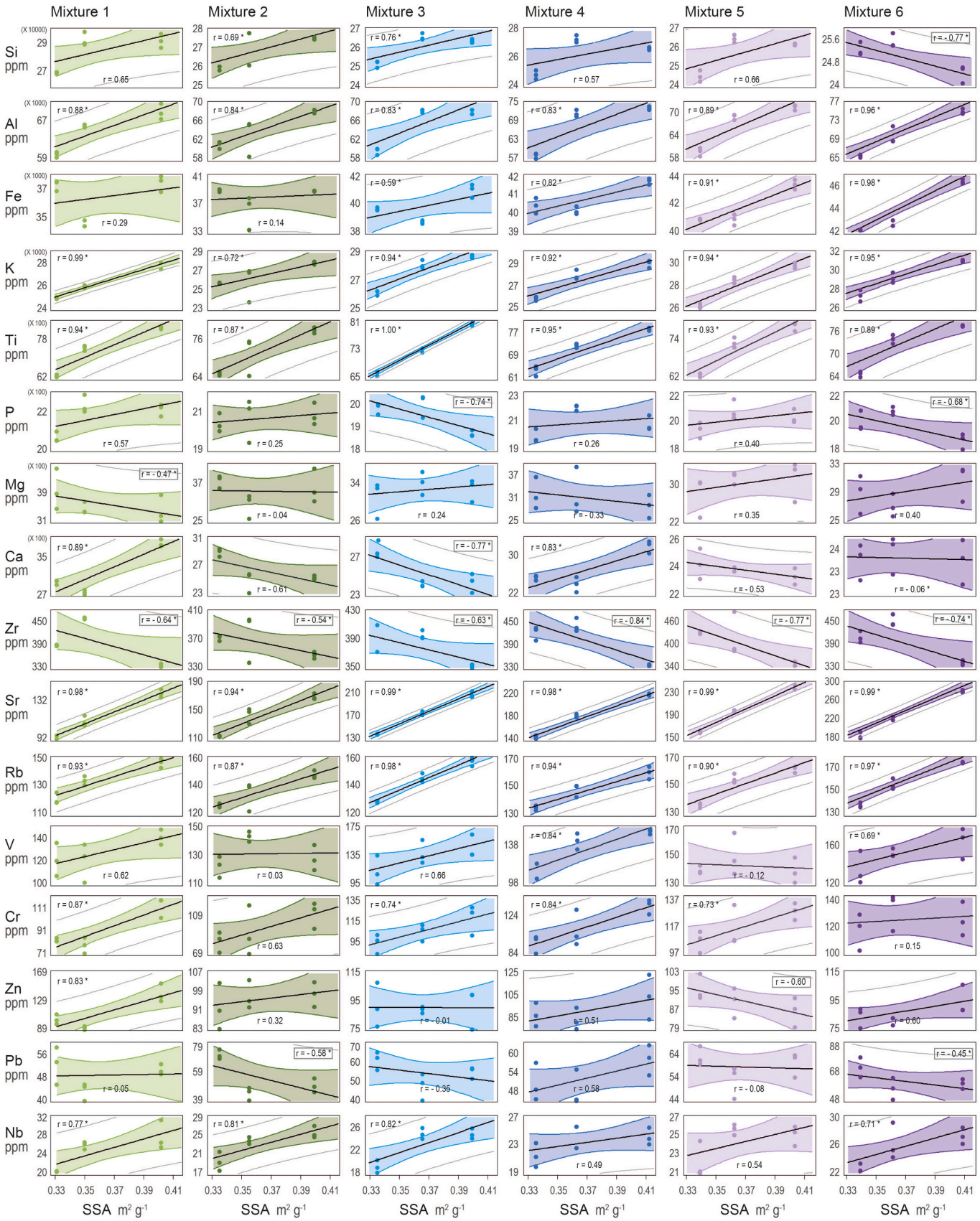


**Fig. 5.** Linear regression models between specific surface area (SSA, $m^2\ g^{-1}$) and element contents (ppm) for each experimental mixture. Each model shows the line of best least squares fit (black line) together with the confidence intervals for the mean response at SSA (color lines) and the prediction limits for new observations (grey lines). (For interpretation of the references to color in this figure legend, the reader is referred to the web version of this article.)

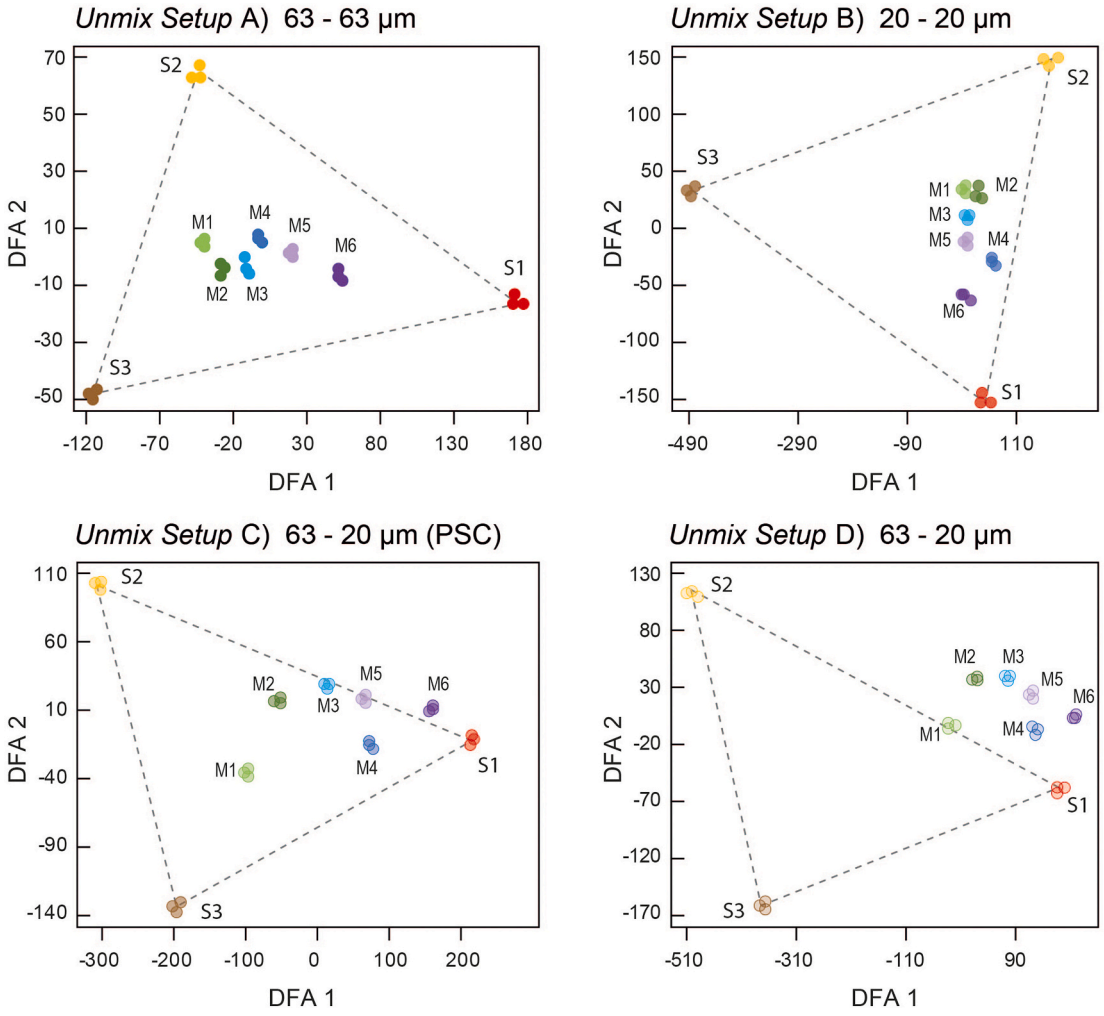


**Fig. 6.** Two-dimensional scatterplots of the first and second discriminant functions from stepwise discriminant function analysis for each unmix setup (A, B, C and D).

Our results show that the specific surface area of fractionated sediment parcels exerts a primary influence upon the analysed concentration of most elements. In this respect, the scatterplots and regression models obtained for the source and mixture samples, respectively (Figs. 4 and 5), illustrate the control of particle size fraction on the elemental content and suggest that the relation between SSA and content is different for each element in terms of linearity, magnitude and even direction, and it also depends on the type of sample.

When comparing fractions <63, <40 and <20 µm with 63–40 and 40–20 µm, an attenuation of the particle size factor effect occurs because more grain sizes are included in the ranges fractions and the expected effect of enrichment in fine fractions could be weakened.

The size-fractionated samples have higher concentrations of most elements in the finer fractions. It is widely accepted that the smaller particles are more chemically reactive and, therefore, concentrate geochemical elements, reflecting an increase of the elemental adsorption by the soil particles with higher SSA (Acosta et al., 2011). However, a notable exception is Zr, which, as commented above, concentrates most in the coarser fractions that could be related with detrital zircon as found by Castillo et al. (2008). More information on the sources might help understand Zr behaviour with important insights in mineralogical and weathering controls.

### 4.2. Unmixing model

There is no standard combination of statistical methods to select the composite tracers in sediment tracing and there is abundant literature showing the effect of tracer selection methods in unmixing results (e.g. Palazón et al., 2015; Lizaga et al., 2020c). In our experimental study the two different sets of tracers based on RT or the combination of RT, KW and DFA, also indicate some differences in the estimated source apportions suggesting an effect on the model.

Our results demonstrate that for the setup A (63–63 µm) higher difference between estimates of source apportions is recorded when only the range test is applied. However, the opposite was observed for setups B, C and D; when a larger number of tracers by using RT instead the three tests provided much better results demonstrating the sensitivity of the model predictions to the selection of different tracers. In this regard, recent studies have proposed novel methodologies for selecting the optimum set of tracers identifying non-conservative and dissenting tracers which is model independent (Lizaga et al., 2020c), and its application has provided meaningful results (Navas et al., 2020).

Applying different statistic tests reveals a remarkable difference in the bunch of elements selected as optimum tracers. The range test selected as many as 16 optimum tracers (Table 5), including elements associated with both the silt and clay fractions (Fig. 3). However, the only three elements (Rb, K, Sr) selected after applying the three tests are exclusively linked to the silt fraction. In general, even if the model outputs with the three tracers generates less variability in the sources contributions, it could be a bias effect triggered by the components in the silt fraction that increases the most in the <20 µm fraction. This could be the reason why apart from setup A, the model results do not

**Table 5**
Optimum fingerprint tracers obtained with the assessed statistical tests: i) Range test and ii) Range test, Kruskal Wallis test and DFA test for each of mixture and unmix setup.

| Mixtures | Unmix setups | i) Range test | | ii) Range test, KW, DFA | |
|---|---|---|---|---|---|
| | | n | | n | |
| Mix 1 | A | 16 | Si, Al, Fe, K, Ti, P, Mg, Ca, Zr, Sr, Rb, V, Cr, Zn, Pb, Nb | 3 | K, Sr, Rb |
| | B | 15 | Si, Al, Fe, K, Ti, P, Mg, Ca, Zr, Sr, Rb, V, Cr, Zn, Pb | 3 | K, Sr, Rb |
| | C | 13 | Si, Al, K, Ti, P, Mg, Ca, Sr, Rb, V, Cr, Zn, Pb | 3 | K, Sr, Rb |
| | D | 13 | Al, Fe, K, P, Mg, Ca, Zr, Sr, Rb, V, Cr, Zn, Pb | 3 | K, Sr, Rb |
| Mix 2 | A | 15 | Si, Al, Fe, K, Ti, P, Mg, Ca, Zr, Sr, Rb, V, Cr, Zn, Nb | 3 | K, Sr, Rb |
| | B | 15 | Si, Al, Fe, K, Ti, P, Mg, Ca, Sr, Rb, V, Cr, Zn, Pb, Nb | 3 | K, Sr, Rb |
| | C | 14 | Si, Al, K, Ti, P, Mg, Ca, Sr, Rb, V, Cr, Zn, Pb, Nb | 3 | K, Sr, Rb |
| | D | 13 | Al, Fe, K, P, Mg, Ca, Zr, Sr, Rb, V, Cr, Zn, Pb | 3 | K, Sr, Rb |
| Mix 3 | A | 16 | Si, Al, Fe, K, Ti, P, Mg, Ca, Zr, Sr, Rb, V, Cr, Zn, Pb, Nb | 3 | K, Sr, Rb |
| | B | 15 | Si, Al, Fe, K, Ti, P, Mg, Ca, Sr, Rb, V, Cr, Zn, Pb, Nb | 3 | K, Sr, Rb |
| | C | 14 | Si, Al, K, Ti, P, Mg, Ca, Sr, Rb, V, Cr, Zn, Pb, Nb | 3 | K, Sr, Rb |
| | D | 13 | Si, Al, Fe, K, P, Mg, Ca, Zr, Sr, Rb, Cr, Zn, Pb | 3 | K, Sr, Rb |
| Mix 4 | A | 16 | Si, Al, Fe, K, Ti, P, Mg, Ca, Zr, Sr, Rb, V, Cr, Zn, Pb, Nb | 3 | K, Sr, Rb |
| | B | 16 | Si, Al, Fe, K, Ti, P, Mg, Ca, Zr, Sr, Rb, V, Cr, Zn, Pb, Nb | 3 | K, Sr, Rb |
| | C | 14 | Si, Al, K, Ti, P, Mg, Ca, Sr, Rb, V, Cr, Zn, Pb, Nb | 3 | K, Sr, Rb |
| | D | 14 | Si, Al, Fe, K, P, Mg, Ca, Zr, Sr, Rb, V, Cr, Zn, Pb | 3 | K, Sr, Rb |
| Mix 5 | A | 14 | Si, Al, Fe, K, Ti, P, Mg, Ca, Zr, Sr, Rb, V, Cr, Zn | 3 | K, Sr, Rb |
| | B | 15 | Si, Al, Fe, K, Ti, P, Mg, Ca, Sr, Rb, V, Cr, Zn, Pb, Nb | 3 | K, Sr, Rb |
| | C | 14 | Si, Al, K, Ti, P, Mg, Ca, Sr, Rb, V, Cr, Zn, Pb, Nb | 3 | K, Sr, Rb |
| | D | 14 | Si, Al, Fe, K, P, Mg, Ca, Zr, Sr, Rb, V, Cr, Zn, Pb | 3 | K, Sr, Rb |
| Mix 6 | A | 15 | Si, Al, Fe, K, Ti, P, Mg, Ca, Zr, Sr, Rb, V, Cr, Zn, Nb | 3 | K, Sr, Rb |
| | B | 15 | Si, Al, Fe, K, Ti, P, Mg, Ca, Sr, Rb, V, Cr, Zn, Pb, Nb | 3 | K, Sr, Rb |
| | C | 13 | Al, Fe, K, Ti, Mg, Ca, Sr, Rb, V, Cr, Zn, Pb, Nb | 3 | K, Sr, Rb |
| | D | 11 | Si, Fe, K, P, Mg, Ca, Zr, Sr, Cr, Zn, Pb | 2 | K, Sr |

adjust so well to the theoretical contributions for setups C and D (AE range C: 2.6–27.3 and AE range D: 5.8–40.4) as when the model is applied with a higher number of tracers extracted from the range test (AE range C: 1.9–18.9 and AE range D: 3.1–26.4). By including more tracers associated with both the silt and clay fraction (Table 6), there is greater variability in the sources apportions, but these results turn out to be more averaged and closer to the known contributions.

We found that the most accurate source apportionment results were achieved when comparing source and mixtures with similar grain sizes, especially for the fraction <63 μm (setup A) against <20 μm (setup B). The complexities introduced in this approach by comparing different size fractions between sources and mixtures (set D) are slightly reduced by using particle size correction factor (set C). However, applying corrections to remove source-to-sediment differences could also remove differences in source tracer concentrations that are essential for source discrimination, as it has been evidenced in previous studies (Laceby et al., 2017; Smith et al., 2018). Even though the good discrimination between the different experimental sources and sediments for setup A (Fig. 6), the effect of fine particle size likely limited the capabilities for better discrimination, especially in setup D, influencing the model results.

**Table 6**
Values of goodness of fit (GOF), root mean squared error (RMSE) and absolute error (AE) of each source contribution predicted by the 4 unmix setups (A, B, C, D) using the composite signatures selected after i) range test and ii) RT, KW and DFA, central value. Table shows the values for the 6 artificial mixtures (mean of the three replicates). Results for the 18 experimental mixtures (6 experimental mixtures with three replicates each: r1, r2, r3) are included in Supplementary material.
4 Setups (source μm – mixtures μm): A) 63–63 μm, B) 20–20 μm, C) 63–20 μm with PSC, D) 63–20 μm without PSC.

| | | i) Range test | | | | | ii) Range test, KW, DFA | | | | |
|---|---|---|---|---|---|---|---|---|---|---|---|
| | | Tracers | RMSE | AE $_{S1}$ | AE $_{S2}$ | AE $_{S3}$ | Tracers | RMSE | AE $_{S1}$ | AE $_{S2}$ | AE $_{S3}$ |
| Mix 1 | A | 16 | 3.0 | 1.2 | 4.1 | 2.9 | 3 | 1.4 | 0.1 | 1.8 | 1.7 |
| | B | 15 | 7.6 | 6.2 | 4.5 | 10.7 | 3 | 13.5 | 3.3 | 14.7 | 17.9 |
| | C | 13 | 9.9 | 11.9 | 0.5 | 12.4 | 3 | 15.0 | 9.9 | 11.3 | 21.2 |
| | D | 13 | 22.1 | 26.1 | 28.0 | 2.0 | 3 | 24.3 | 32.2 | 26.5 | 5.8 |
| Mix 2 | A | 15 | 2.4 | 3.1 | 0.5 | 2.6 | 3 | 0.5 | 0.8 | 0.5 | 0.3 |
| | B | 15 | 8.2 | 4.8 | 11.6 | 6.8 | 3 | 15.8 | 0.4 | 19.1 | 19.6 |
| | C | 14 | 9.8 | 9.3 | 4.3 | 13.6 | 3 | 16.2 | 9.5 | 13.3 | 22.8 |
| | D | 13 | 13.6 | 18.7 | 13.3 | 5.4 | 3 | 23.2 | 32.1 | 22.0 | 10.0 |
| Mix 3 | A | 16 | 4.4 | 2.7 | 3.5 | 6.2 | 3 | 1.3 | 1.8 | 1.4 | 0.5 |
| | B | 15 | 8.2 | 1.1 | 9.5 | 10.6 | 3 | 15.3 | 4.4 | 16.2 | 20.6 |
| | C | 14 | 14.8 | 18.0 | 0.3 | 18.3 | 3 | 17.4 | 18.6 | 4.8 | 23.4 |
| | D | 13 | 11.2 | 15.7 | 6.1 | 9.6 | 3 | 27.6 | 38.4 | 24.7 | 13.7 |
| Mix 4 | A | 16 | 3.1 | 1.2 | 3.0 | 4.3 | 3 | 2.9 | 2.4 | 1.7 | 4.0 |
| | B | 16 | 8.0 | 10.4 | 1.2 | 9.1 | 3 | 14.7 | 5.3 | 14.9 | 20.1 |
| | C | 14 | 15.2 | 21.4 | 9.0 | 12.4 | 3 | 18.5 | 14.0 | 12.2 | 26.1 |
| | D | 14 | 17.4 | 24.6 | 12.9 | 11.5 | 3 | 29.2 | 40.7 | 26.7 | 13.9 |
| Mix 5 | A | 14 | 3.4 | 4.7 | 2.8 | 2.0 | 3 | 3.2 | 0.1 | 3.9 | 3.8 |
| | B | 15 | 5.0 | 0.8 | 6.4 | 5.6 | 3 | 12.7 | 3.2 | 13.7 | 16.9 |
| | C | 14 | 13.2 | 18.4 | 6.3 | 12.1 | 3 | 17.2 | 19.2 | 3.2 | 22.4 |
| | D | 14 | 14.7 | 20.8 | 9.6 | 11.2 | 3 | 29.0 | 40.0 | 28.0 | 12.0 |
| Mix 6 | A | 15 | 2.8 | 0.1 | 3.4 | 3.5 | 3 | 2.4 | 3.4 | 1.3 | 2.1 |
| | B | 15 | 10.7 | 9.7 | 5.1 | 14.8 | 3 | 12.0 | 10.6 | 6.2 | 16.8 |
| | C | 13 | 8.4 | 4.8 | 7.0 | 11.8 | 3 | 21.3 | 27.8 | 3.7 | 24.1 |
| | D | 11 | 9.8 | 13.2 | 10.4 | 2.8 | 2 | 27.7 | 38.6 | 25.0 | 13.6 |

Despite the fact that the RMSE and absolute errors of source apportions for S1 and S2 reduced in most cases when a PSC factor was used, the increase in the AE for S3 in almost 92% of the cases indicates that applying a PSC factor for all tracers indistinctly before the unmixing will not be a fully suitable approach. Our data confirm that fingerprint properties compared between materials with very different particle size characteristics (setups D, C) will need careful examination when applying PSC factor. Albeit the wide use of this particle size correction (Collins et al., 2001; Carter et al., 2003), it has been reported that applying a single PSC factor for all parameters could negatively affect unmixing results (Koiter et al., 2013). For example, Smith and Blake (2014) demonstrated that the hypothesis of positive linearity between particle size and tracer concentration does not apply to all tracer properties.

Our study provides clear evidence that the assumption of linearity should be routinely tested before applying PSC factors for un-mixing. Russell et al. (2001) also demonstrated that the linear particle size correction relationship was inappropriate when there were large SSA differences between sources, while new approaches avoid applying corrections to tracer data for particle size (Smith et al., 2018).

Our results confirm the validity of the general assumption that considers the <63 μm fraction to be adequate for fingerprinting analysis, except for those areas characterised by abundance of very fine silt and clay materials. This is particularly the case in studies performed in Australia in which the <10 μm fraction was predominantly used (Olley and Caitcheon, 2000; Wallbrink, 2004). Research by Motha et al. (2003) indicates that in suspended sediments exclusively composed of <63 μm particle sizes more than 90% of the sediments were <20 μm in size, that was also observed by Collins et al. (1997). In this regard, it would be beneficial for improving fingerprinting results to report summary statistics for particle size data of both sources and sediment mixtures to document this informative comparison in order to scrutinise tracer selection performance when applying the unmixing models.

Despite the limitations and potential uncertainties (associated with the analytical precision of XRF), our findings support the idea that a universal PSC factor for all elements could produce unrepresentative corrections because assumes an enrichment in the finest fraction. We demonstrate that not all elements have a positive correlation with SSA, and accordingly, the use of a PSC factor before the unmixing does not provide accurate apportions to the known source proportions. The more accurate results achieved by comparing source and mixtures with same particle size, especially for <63 μm particle size, suggest that the use of this fraction allows embracing wider information of the elemental composition of samples against the use of <20 μm. The significant

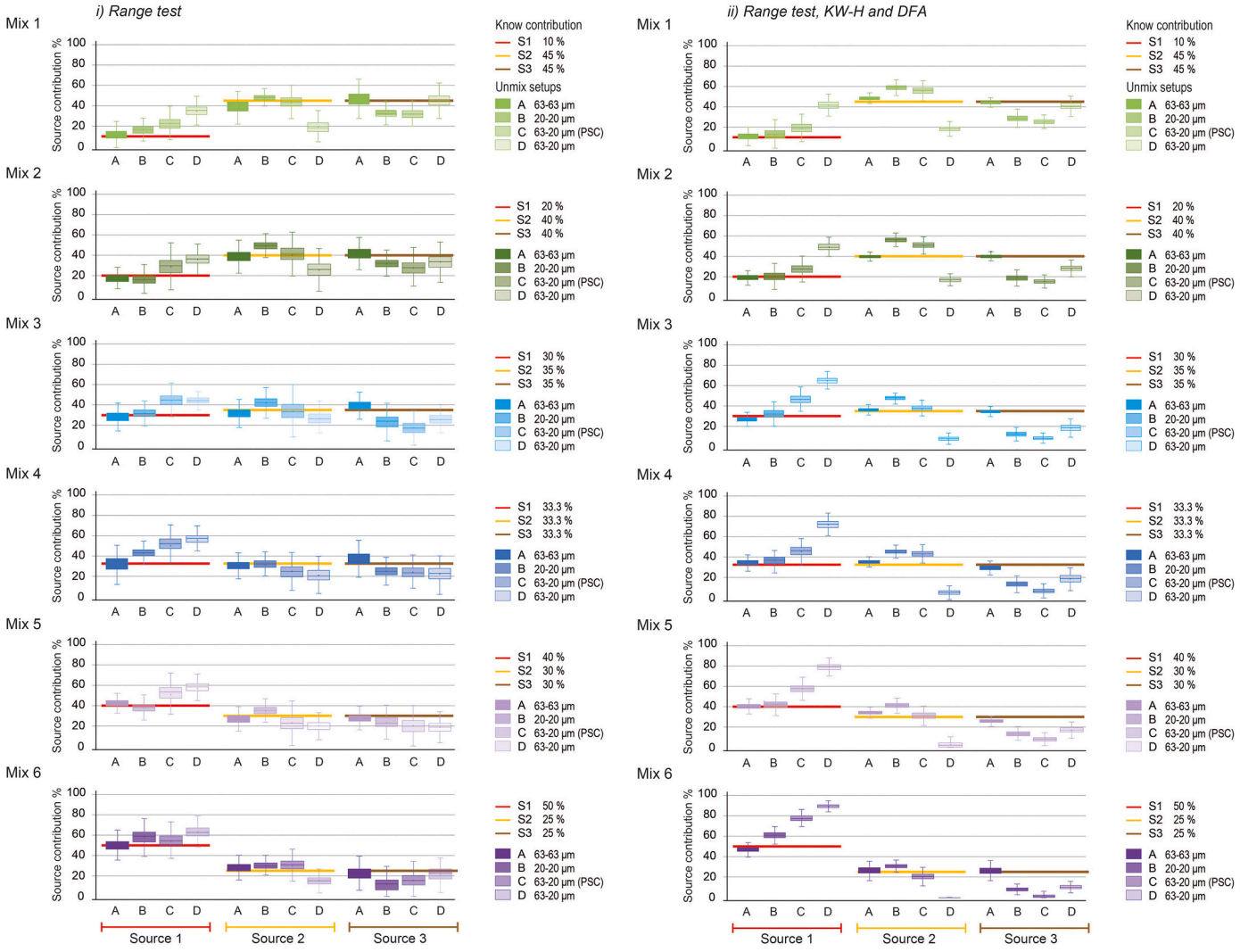


**Fig. 7.** Comparison of the predicted and known relative contributions from the sources to the 6 mixtures (18 experimental mixtures as there are 3 replicates per mixture r1, r2, r3, and 6 artificial mixtures as the mean of the three replicates per mixture) using the composite signatures selected after i) range test and ii) RT, KW and DFA for the 4 unmix setups: A) sources and mixtures at 63 μm, B) sources and mixtures at 20 μm, C) sources at 63 μm and mixtures at 20 μm with particle size correction factor (PSC) and D) sources at 63 μm and mixtures at 20 μm without PSC factor.

increase in fines in <20 μm, especially in silt but not so much in clay, which affects the elemental composition linked to the mineralogy of this fraction, could justify the need of using more number of tracers to obtain more accurate results and avoid biased information. Therefore, it emerges that thorough characterisation of the sources and mixtures would assist for a sound application of correction factors.

The unmixing results confirm that the elements bound to fine sediments either contained in the mineral matrix or adsorbed on mineral surfaces are key drivers governing the geochemistry derived from particle size selectivity. Thus the geochemical fingerprint likely will change if the <2 mm, the <63 μm, or the <10 μm fraction are sampled and analysed (e.g. Gibbs, 1967; Laceby et al., 2017).

Our findings highlight the difficulty to predict the impact of particle size on elemental concentrations and the complexity of the relationship between SSA and elemental geochemistry. The experimental samples in this research from a sedimentary substrate result in similarities between the sources but complexity will likely increase if sources come from highly contrasted parent materials.

## 5. Conclusion

This research provided experimental information which helps to comprehensively characterise the predictability of fingerprint properties when particle size is affected. Even if the experimental design accounted for similar sedimentary substrates, a good source discrimination between the three sources and complex effect of particle size have been evidenced. Our results have demonstrated that the impact of particle size on elemental content is difficult to predict, and the relationships between the specific surface area and elemental geochemistry are specific in terms of the magnitude, direction, and linearity, which suggests that the use of particle size correction factors needs to be given careful consideration.

Based on our findings, a particle size correction factor based on an SSA ratio, and assuming positive linearity between particle size and tracer concentration, may be inappropriate. A single PSC factor for all tracers could negatively affect the final unmixing results. We conclude that a robust analysis of the particle size distribution of the sources and sediment mixtures should be constantly examined before applying unmixing models. Likewise, efforts should be made in future studies to incorporate in unmixing model calculations, the distribution of particle size of source and sediments together with the concentration of the tracers as an alternative to the use of a single particle size correction factor for all fingerprints.

The grain size fraction selected when comparing source and mixtures with similar grain size distribution influences the source apportionment results. We found that the most accurate source apportionment results were achieved by comparing sources and mixtures with the <63 μm grain-size fraction, while when <20 μm were compared higher deviation of the known apportions was recorded. Our findings provide evidence to support that the source apportionment results estimated by the unmixing model are sensitive to particle size but also to tracer selection. Benefits have been observed by including more tracers when there are large differences in grain size (SSA) between sources and mixtures, or when very fine sources and mixtures are compared. Results of this research can be used to guide the particle size correction factors based on SSA and the interpretation of apportionment results.

Supplementary data to this article can be found online at https://doi.org/10.1016/j.geomorph.2022.108178.

## Declaration of competing interest

The authors declare that they have no known competing financial interests or personal relationships that could have appeared to influence the work reported in this paper.

## Acknowledgment

This research has been supported by projects PID2019-103946RJ-I00 and PID2019-104857RB-I00 funded by the Spanish Ministry of Science and Innovation (State Research Agency).

## References

Acosta, J.A., Faz, A., Kalbitz, K., Jansen, B., Martinez-Martinez, S., 2011. Heavy metal concentrations in particle size fractions from street dust of Murcia (Spain) as the basisfor risk assessment. J. Environ. Monit. 13, 3087–3096.
Blake, W.H., Ficken, K.J., Taylor, P., Russell, M.A., Walling, D.E., 2012. Tracing crop-specific sediment sources in agricultural catchments. Geomorphology 140, 322–329.
Blake, W.H., Boeckx, P., Stock, B.C., Smith, H.G., Bodé, S., Upadhayay, H.R., Gaspar, L., Goddard, R., Lennard, A.T., Lizaga, I., Lobb, D.A., Owens, P.N., Petticrew, E.L., Kuzyk, Z.Z.A., Gari, B.D., Munishi, L., Mtei, K., Nebiyu, A., Mabit, L., Navas, A., Semmens, B.X., 2018. A deconvolutional Bayesian mixing model approach for river basin sediment source apportionment. Sci. Rep. 8, 13073.
Carter, J., Owens, P.N., Walling, D.E., Leeks, G.J.L., 2003. Fingerprinting suspended sediment sources in a large urban river system. Sci. Total Environ. 314–316, 513–534.
Castillo, S., Moreno, T., Querol, X., et al., 2008. Trace element variation in size-fractionated African desert dusts. J. Arid Environ. 1, 1031–1042.
Collins, A.L., Walling, D.E., Leeks, G.J.L., 1997. Source type ascription for fluvial suspended sediment based on a quantitative composite fingerprinting technique. Catena 29, 1–27.
Collins, A.L., Walling, D.E., Sichingabula, H.M., Leeks, G.J.L., 2001. Suspended sediment source fingerprinting in a small tropical catchment and some management implications. Appl. Geogr. 21 (4), 387–412.
Collins, A.L., Zhang, Y., McChesney, D., Walling, D.E., Haley, S.M., Smith, P., 2012. Sediment source tracing in a lowland agricultural catchment in southern England using a modified procedure combining statistical analysis and numerical modelling. Sci. Total Environ. 414, 301–317.
Collins, A.L., Pulley, S., Foster, I.D.L., Gellis, A., Porto, P., Horowitz, A.J., 2017. Sediment source fingerprinting as an aid to catchment management a review of the current state of knowledge and a methodological decision-tree for end-users. J. Environ. Manag. 194, 86–108.
Collins, A.L., Blackwell, M., Boeckx, P., Chivers, C.A., Emelko, M., Evrard, O., Foster, I., Gellis, A., Gholami, H., Granger, S., Harris, P., Horowitz, A.J., Laceby, J.P., Martinez-Carreras, N., Minella, J., Mol, L., Nosrati, K., Pulley, S., Silins, U., Jacques da Silva, Y., Stone, M., Tiecher, T., Upadhayay, H.R., Zhang, Y., 2020. Sediment source fingerprinting: benchmarking recent outputs, remaining challenges and emerging themes. J. Soils Sediments 20, 4160–4193.
Douglas, G., Palmer, M., Caitcheon, G., 2003. The provenance of sediments in Moreton Bay, Australia: a synthesis of major, trace element and Sr-Nd-Pb isotopic geochemistry, modelling and landscape analysis. Hydrobiologia 494, 145–152.
Foster, I.D.L., Lees, J.A., Owens, P.N., Walling, D.E., 1998. Mineral magnetic characterization of sediment sources from an analysis of lake and floodplain sediments in the catchments of Old Mill Reservoir and Slapton Ley, South Devon,UK. Earth Surf. Process. Landf. 23, 685–703.
Foucher, A., Laceby, P.J., Salvador-Blanes, S., Evrard, O., Le Gall, M., Lefèvre, I., Cerdan, O., Rajkumar, V., Desmet, M., 2015. Quantifying the dominant sources of sediment in a drained lowland agricultural catchment: the application of a thorium-based particle size correction in sediment fingerprinting. Geomorphology 250, 271–281.
Gaspar, L., Lizaga, I., Blake, W.H., Latorre, B., Quijano, L., Navas, A., 2019a. Fingerprinting changes in source contribution for evaluating soil response during an exceptional rainfall in Spanish pre-pyrenees. J. Environ. Manag. 240, 136–148.
Gaspar, L., Blake, W.H., Smith, H.G., Lizaga, I., Navas, A., 2019b. Testing the sensitivity of a multivariate mixing model using geochemical fingerprints with artificial mixtures. Geoderma 337, 498–510.
Gholami, H., TakhtiNajad, E.J., Collins, A.L., Fathabadi, A., 2019. Monte Carlo fingerprinting of the terrestrial sources of different particle size fractions of coastal sediment deposits using geochemical tracers: some lessons for the user community. Environ. Sci. Pollut. Res. 26, 13560–13579.
Gibbs, R.J., 1967. Amazon river system: environmental factors that control its dissolved and suspended load. Science 156, 1734–1737.
Guagliardi, I., Apollaro, C., Scarciglia, F., De Rosa, R., 2013. Influence of particle-size on geochemical distribution of stream sediments in the Lese river catchment, southern Italy. Biotechnol. Agron. Soc. Environ. 17 (1), 43–55.
Haddadchi, A., Olley, J., Pietsch, T., 2015. Quantifying sources of suspended sediment in three size fractions. J. Soils Sediments 15, 2086–2100.
Hatfield, R.G., Maher, B.A., 2009. Fingerprinting upland sediment sources: particle size-specific magnetic linkages between soils, lake sediments and suspended sediments. Earth Surf. Process. Landf. 34, 1359–1373.
Horowitz, A.J., 1991. A Primer on Sediment-trace Element Chemistry, 2nd ed. Lewis Publishers, Chelsea, Michigan, USA.
Horowitz, A.J., Elrick, K.A., 1987. The relation of stream sediment surface area, grain size and composition to trace element chemistry. Appl. Geochem. 2, 437–451.
Koiter, A.J., Owens, P.N., Petticrew, E.L., Lobb, D.A., 2013. The behavioural characteristics of sediment properties and their implications for sediment fingerprinting as an approach for identifying sediment sources in river basins. Earth-Sci. Rev. 125, 24–42.

Koiter, A.J., Owens, P.N., Petticrew, E.L., Lobb, D.A., 2018. Assessment of particle size and organic matter correction factors in sediment source fingerprinting investigations: an example of two contrasting watersheds in Canada. Geoderma 325, 195–207.
Laceby, J.P., Evrard, O., Smith, H.G., Blake, W.H., Olley, J.M., Minella, J.P.G., Owens, P. N., 2017. The challenges and opportunities of addressing particle size effects in sediment source fingerprinting: a review. Earth-Sci. Rev. 169, 85–103.
Lizaga, I., Gaspar, L., Latorre, I., Navas, A., 2020a. Variations in transport of fine sediment and associated elements induced by rainfall and agricultural cycle in a Mediterranean agroforestry catchment. J. Environ. Manag. 111020.
Lizaga, I., Latorre, B., Gaspar, L., Navas, A., 2020b. FingerPro: an R package for tracking the provenance of sediment. Water Resour. Manag. 34 (12), 3879–3894.
Lizaga, I., Latorre, B., Gaspar, L., Navas, A., 2020c. Consensus ranking as a method to identify non-conservative and dissenting tracers in fingerprinting studies. Sci. Total Environ. 720, 137537.
Lizaga, I., Bodé, S., Gaspar, L., Latorre, L., Boeckx, P., Navas, A., 2021. Legacy of historic land cover changes on sediment provenance tracked with isotopic tracers in a Mediterranean agroforestry catchment. J. Environ. Manag. 288, 112291.
Mandzhieva, S., Minkina, T., Pinskiy, D., Bauer, T., Sushkova, S., 2014. The role of soil's particle-size fractions in the adsorption of heavy metals. Eurasian J. Soil Sci. 3, 197–205.
Mohammadi Raigani, Z., Nosrati, K., Collins, A.L., 2019. Fingerprinting sub-basin spatial sediment sources in a large iranian catchment under dry-land cultivation and rangeland farming: combining geochemical tracers and weathering indices. J. Hydrol. Reg. Stud. 24, 100613.
Motha, J.A., Wallbrink, P.J., Hairsine, P.B., Grayson, R.B., 2002. Tracer properties of eroded sediment and source material. Hydrol. Process. 16, 1983–2000.
Motha, J., Wallbrink, P., Hairsine, P., Grayson, R., 2003. Determining the sources of suspended sediment in a forested catchment in south-eastern Australia. Water Resour. Res. 39, 1056.
Navas, A., Lindhorfer, H., 2003. Geochemical speciation of heavy metals in semiarid soils of the central Ebro valley (Spain). Environ. Int. 29, 61–68.
Navas, A., Lindhorfer, H., 2005. Chemical partitioning of Fe, Mn, Zn and Cr in mountain soils of the Iberian and Pyrenean ranges (NE Spain). Soil Sediment Contam. 14 (3), 249–259.
Navas, A., Valero-Garcés, B.L., Gaspar, L., Machín, J., 2009. Reconstructing the history of sediment accumulation in the Yesa reservoir: an approach for management of mountain reservoirs. Lake Reserv. Manag. 25 (1), 15–27.
Navas, A., Valero-Garcés, B.L., Gaspar, L., Palazón, L., Machín, J., 2011. Radionuclides and stable elements in the sediments of the Yesa reservoir (central Spanish Pyrenees). J. Soils Sediments 11, 1082–1098.
Navas, A., Lizaga, I., Gaspar, L., Latorre, B., Dercon, G., 2020. Unveiling the provenance of sediments in the moraine complex of Aldegonda Glacier (Svalbard) after glacial retreat using radionuclides and elemental fingerprints. Geomorphology 367, 107304.
Nosrati, K., Collins, A.L., Madankan, M., 2018. Fingerprinting sub-basin spatial sediment sources using different multivariate statistical techniques and the Modified MixSIR model. Catena 164, 32–43.
Nosrati, K., Fathi, Z., Collins, A.L., 2019. Fingerprinting sub-basin spatial suspended sediment sources by combining geochemical tracers and weathering indices. Environ. Sci. Pollut. Res. 26, 28401–28414.
Nosrati, K., Akbari-Mahdiabad, M., Fiener, P., Collins, A.L., 2021. Using different size fractions to source fingerprint fine-grained channel bed sediment in a large drainage basin in Iran. Catena 200, 105173.
Olley, J., Caitcheon, G., 2000. Major element chemistry of sediments from the Darling-Barwon river and its tributaries: implications for sediment and phosphorus sources. Hydrol. Process. 14, 1159–1175.
Palazón, L., Latorre, B., Gaspar, L., Blake, W.H., Smith, H.G., Navas, A., 2015. Comparing catchment sediment fingerprinting procedures using an autoevaluation approach with virtual sample mixtures. Sci. Total Environ. 532, 456–466.
Palazón, L., Latorre, B., Gaspar, L., Blake, W.H., Smith, H.G., Navas, A., 2016. Combining catchment modelling and sediment fingerprinting to assess sediment dynamics in a Spanish Pyrenean river system. Sci. Total Environ. 569, 1136–1148.
Pulley, S., Collins, A.L., 2018. Tracing catchment fine sediment sources using the new SIFT (SedIment Fingerprinting Tool) open source software. Sci. Total Environ. 635, 838–858.
Reiffarth, D.G., Petticrew, E.L., Owens, P.N., Lobb, D.A., 2016. Sources of variability in fatty acid (FA) biomarkers in the application of compound-specific stable isotopes (CSSIs) to soil and sediment fingerprinting and tracing: a review. Sci. Total Environ. 565, 8–27.
Russell, M.A., Walling, D.E., Hodgkinson, R.A., 2001. Suspended sediment sources in two small lowland agricultural catchments in the UK. J. Hydrol. 252, 1–24.
Smith, H.G., Blake, W.H., 2014. Sediment fingerprinting in agricultural catchments: a critical re-examination of source discrimination and data corrections. Geomorphology 204, 177–191.
Smith, H.G., Singh Karam, D., Lennard, A.T., 2018. Evaluating tracer selection for catchment sediment fingerprinting. J. Soils Sediments 18, 3005–3019.
Uber, M., Legout, C., Nord, G., Crouzet, C., Demory, F., Poulenard, J., 2019. Comparing alternative tracing measurements and mixing models to fingerprint suspended sediment sources in a mesoscale Mediterranean catchment. J. Soils Sediments 19, 3255–3273.
Wallbrink, P.J., 2004. Quantifying the erosion processes and land-uses which dominate fine sediment supply to Moreton Bay, Southeast Queensland, Australia. J. Environ. Radioact. 76, 67–80.
Walling, D.E., 1998. Erosion and sediment yield research-some recent perspectives. J. Hydrol. 100, 113–141.
Walling, D.E., Woodward, J.C., Nicholas, A.P., 1993. A multi-parameter approach to fingerprinting suspended-sediment sources. In: Peters, N.E., Hoehn, E., Leibundgut, C., Tase, N., Walling, D.E. (Eds.), Tracers in Hydrology, IAHS Publication No. 215. IAHS Press, Wallingford, pp. 329–338.
Walling, D.E., Owens, P.N., Waterfall, B.D., Leeks, G.J., Wass, P.D., 2000. The particle size characteristics of fluvial suspended sediment in the Humber and Tweed catchments,UK. Sci. Total Environ. 251, 205–222.
Wilcke, W., Mosbach, J., Kobza, J., Zech, W., 1998. Distribution of Al and heavy metals in bulk soil and aggregates at three sites contaminated by the emissions of a central Slovak Al smelter. Water Air Soil Pollut. 106, 389–402.
Wu, Y., Zheng, Y., 2004. Genesis of zircon and its constraints on interpretation of U-Pb age. Chin. Sci. Bull. 49, 1554–1569.